



Kinetic analysis of the hydrogen electrode reaction in unbuffered media. Theory and studies on Pt microelectrodes



Mauricio D. Arce¹, Horacio L. Bonazza, José L. Fernández*,¹

Programa de Electroquímica Aplicada e Ingeniería Electroquímica (PRELINE), Facultad de Ingeniería Química, Universidad Nacional del Litoral, Santiago del Estero 2829 (S3000AOM), Santa Fe, Santa Fe, Argentina

ARTICLE INFO

Article history:

Received 22 March 2013

Received in revised form 22 May 2013

Accepted 25 May 2013

Available online xxxx

Keywords:

Hydrogen evolution

Hydrogen oxidation

Water dissociation

Microelectrodes

ABSTRACT

The hydrogen electrode reaction (HER) in steady state was described through a model involving mechanistic, mass-transport, and acid-base events. The model can be used to analyze polarization curves at any pH in conditions of high ionic strength and to obtain from these dependences the complete set of kinetic parameters. On the one hand, it involves the Volmer–Heyrovsky–Tafel (VHT) mechanism with H⁺ and H_{2(dis)} at the electrode surface. On the other hand, the reaction of water dissociation at equilibrium is simultaneously considered as a source of H⁺ and HO⁻. The mass-transport by diffusion of H_{2(dis)}, H⁺ and HO⁻ is included. In conditions of high mass-transport rates where kinetics plays an important role, the equations are able to reproduce the typical features that are observed in experimental current–potential curves in neutral and acid solutions (pH < 8). Besides, they can be used to analyze the dependence of the polarization resistance on the H⁺ concentration over this pH range. From these dependences, the elementary kinetic parameters of the VHT mechanism can be obtained, as it was demonstrated in this work on platinum microelectrodes.

© 2013 Elsevier Ltd. All rights reserved.

1. Introduction

The hydrogen electrode reaction (HER) involves molecular hydrogen being evolved in the cathodic branch (known as the hydrogen evolution reaction or *her*) and oxidized in the anodic branch (known as the hydrogen oxidation reaction or *hor*). Due to its technological relevance, this reaction has been deeply investigated during the last decades. The design and development of new efficient electrocatalysts is largely based on a proper description of the reaction mechanism and on an accurate quantification of its kinetic parameters. The most valuable and reliable tool for carrying out these studies still is the analysis of the experimental dependences of the electrode current on the potential and on other operative variables (pH, hydrogen pressure, temperature, etc.). The more complete the theoretical description of the reaction, the higher is the accuracy of the analysis. Thus, theoretical models describing the complete functionality of the current on the potential and on the other experimental variables are very valuable for this type of analysis.

It is generally assumed that the HER proceeds by Eq. (1) in alkaline media and by Eq. (2) in acid media [1–3].



These two reactions are usually analyzed in conditions of extreme acidity or alkalinity, and different kinetic parameters are measured on a certain electrode material (i.e. Pt) in very acid [4–6] and very basic media [7–9]. In fact, the reaction given by Eq. (1) is a combination of Eq. (2) with the chemical dissociation of water given by Eq. (3).



Under extreme pH conditions, as the concentration of H⁺ or HO⁻ is several orders of magnitude larger than the water dissociation product, it is unnecessary to take into account Eq. (3), but just Eq. (1) or Eq. (2).

The earliest reports on the effects of water dissociation on electrode reactions involving protons were done by Albery. One of these works [10] reported a theoretical analysis concluding that the influence of reaction (3) should be important when the proton concentration is ~10⁻⁴ M or smaller. Therefore, there should be a domain of pH values where the HER is significantly affected both by the rate of the electron-transfer reaction (Eq. (1) or (2))

* Corresponding author. Tel.: +54 342 4571164x2519.

E-mail address: jlfernan@fiq.unl.edu.ar (J.L. Fernández).

¹ ISE member.

and by the rate of the chemical dissociation of water through Eq. (3). A number of more recent reports [11–17] confirmed these theoretical predictions and investigated these effects on the HER under different mass-transport conditions in simple kinetic scenarios. For example, recent works from Mayrhofer and co-workers analyzed the modification of surface pH during the HER and its effects on the current-potential curves over a low-current interval [11,12]. They assumed that both reactions (2) and (3) were at equilibrium and thus the HER operated under mass-transport control on rotating disk electrodes (RDEs). In near neutral conditions the polarization curves show a cathodic constant current due to mass transport of H⁺ (pH < 7) or an anodic constant current due to mass transport of HO⁻ (pH > 7). This last one occurs before the pH-independent anodic limiting current due to mass transport of dissolved H₂ is reached.

The *her* has also been studied in solutions of low acidity (pH > 2) under conditions of high mass-transport rates, such as those established on microelectrodes [16–18]. The cathodic constant current is observed when the H⁺ concentration is low enough and/or the rate of mass transport is sufficiently high to avoid nucleation of H₂ bubbles on the electrode surface. As long as the source of H⁺ is a strong acid and the ionic strength of the solution is high, the dependence of the cathodic constant current with the concentration of H⁺ follows the theoretical laws of diffusive mass transport [17,18]. This constant current is sustained over a pH-dependant potential range, which becomes narrower for increasing pH values. Upon going to more negative potentials the current starts increasing due to reaction (3). The effects of many factors on these curves were analyzed, such as mass transport by migration in solutions with low ionic strength [13,17] and the use of weak acids as proton sources [15–17,19]. However, the effects of the kinetic parameters on these dependences were not analyzed yet.

Under experimental conditions of high mass-transport rates, the assumption that the HER is infinitely rapid may not be a valid approximation, even on Pt [6]. In these cases, the kinetic parameters of the HER mechanism should be taken into account to model the polarization curves, in addition to the contributions of the changes of local pH and of reaction (3). To contribute to the description of this reaction under these conditions, this work presents an analysis of the HER occurring on microelectrodes through the VHT mechanism including mass transport of protons and of dissolved hydrogen and the water dissociation reaction. First we examine the descriptive capabilities of the model and the sensitivity of the kinetic parameters to the expected responses, with the goal to identify potential applications of the model for calculation of these parameters. Thus, the equations were used to simulate polarization curves over the complete potential range at any pH and the dependence of the polarization resistance (R_p) on the concentration of protons. Finally, we demonstrate the usefulness of the model to extract kinetic parameters of the HER reaction mechanism on Pt from polarization curves measured at different un-buffered solutions on micrometer-sized microelectrodes.

2. Theory

2.1. Mass-transport model

The model assumes a reaction scheme similar to that presented in previous reports [11–14], where the HER proceeds by discharge of H⁺ (or hydronium ions) through reaction (2). In acid media, the only sources of H⁺ that fix the bulk concentration of H⁺ ($c_{\text{H}^+}^*$) are the strong acid that is present in the electrolyte and the water molecules through reaction (3), which is considered at equilibrium. In alkaline solutions, $c_{\text{H}^+}^*$ is indirectly adjusted by a strong base through reaction (3). The bulk concentration of dissolved H₂ ($c_{\text{H}_2}^*$)

is fixed by the partial pressure of saturating H₂. As the model is conceived to be used on microelectrodes, the reaction occurs in steady state in quiescent solutions with an excess of supporting electrolyte that keeps the ionic strength constant at a high value. It is assumed that H₂ bubbles are not formed during the *her* due to oversaturation at the electrode surface [2,20] and a fast transport of dissolved H₂ from the electrode surface [17,18]. Thus, the mass-transport mechanisms by migration and convection are neglected, being diffusion the only mechanism for the transportation of reactants and products from/toward the electrode surface. As the concentrations of H⁺ and HO⁻ are affected not only by the mass transport but also by reaction (3), only the diffusion of dissolved H₂ is handled through the model of the Nernst diffusion layer [21], which assumes a linear gradient of dissolved-H₂ concentration across a diffusion layer with thickness δ . As it is detailed in Appendix A, this model leads to the relationship between the current density (j) and the surface concentration of H⁺ (C_{H^+}) normalized respect to $c_{\text{H}^+}^*$ ($C_{\text{H}^+} = c_{\text{H}^+}/c_{\text{H}^+}^*$) given by Eq. (4), where the parameters ξ , ψ , and $j_{L,a}$ (anodic limiting current density, limited by mass transport of dissolved H₂) are defined as $\xi = D_{\text{H}^+}c_{\text{H}^+}^*/(2D_{\text{H}_2}c_{\text{H}_2}^*)$, $\psi = D_{\text{HO}^-}K_w/(D_{\text{H}^+}c_{\text{H}^+}^{*2})$, $j_{L,a} = 2FD_{\text{H}_2}c_{\text{H}_2}^*/\delta$.

$$\frac{j}{j_{L,a}} = -\xi \left[(1 - C_{\text{H}^+}) + \psi \left(\frac{1}{C_{\text{H}^+}} - 1 \right) \right] \quad (4)$$

This dependence is identical to that reported in recent works from Mayrhofer et al. [11,12], which was obtained by assuming an effective diffusion layer thickness that averaged the contributions of H⁺ and HO⁻. Even though the descriptive capability of the Eq. (4) was fully analyzed by Mayrhofer et al. [11] over low-current intervals, we present a short discussion that focuses the analysis over the whole polarization curves to identify aspects that will be relevant for the kinetic study of the HER. It should be remarked that the parameter ψ is the key factor that governs the effect of the solution pH on the current-potential dependences. Particularly, the appearance of cathodic and anodic constant currents observed over a range of near-neutral pH conditions can be predicted for certain values of ψ .

The $j(C_{\text{H}^+})$ dependences calculated from Eq. (4) over wide ranges of c_{H^+} and $c_{\text{H}^+}^*$ are plotted in Fig. 1a (acid solutions) and b (alkaline solutions), assuming reported values for diffusion coefficients and solubility of H₂ ($D_{\text{H}^+} = 9.3 \times 10^{-5} \text{ cm}^2 \text{s}^{-1}$, $D_{\text{HO}^-} = 5.3 \times 10^{-5} \text{ cm}^2 \text{s}^{-1}$, $D_{\text{H}_2} = 3.7 \times 10^{-5} \text{ cm}^2 \text{s}^{-1}$, $c_{\text{H}_2}^* = 7.1 \times 10^{-7} \text{ mol cm}^{-3}$) [11]. As it was demonstrated in previous analyses and in accordance with experimental evidence [11–18,22], the curves in Fig. 1a indicate that in acid conditions the *her* current density reaches a constant value limited by the diffusion of H⁺ (j_{H^+}). From the analysis of Eq. (4), a constant cathodic current defined by Eq. (5) is attained only when $\psi \ll C_{\text{H}^+} \ll 1$.

$$j_{\text{H}^+} = -\frac{FD_{\text{H}^+}c_{\text{H}^+}^*}{\delta} = -\xi j_{L,a}; \quad \psi \ll C_{\text{H}^+} \ll 1 \quad (5)$$

On the other hand, in slightly alkaline solutions the *hor* tends to reach a constant value smaller than $j_{L,a}$, that is controlled by the diffusion of HO⁻ (j_{HO^-}), as can be seen in Fig. 1b. This constant current is given by Eq. (6), which is obtained from Eq. (4) when $1 \ll C_{\text{H}^+} \ll \psi$.

$$j_{\text{HO}^-} = \frac{FD_{\text{HO}^-}c_{\text{HO}^-}^*}{\delta} = \xi \psi j_{L,a}; \quad 1 \ll C_{\text{H}^+} \ll \psi \quad (6)$$

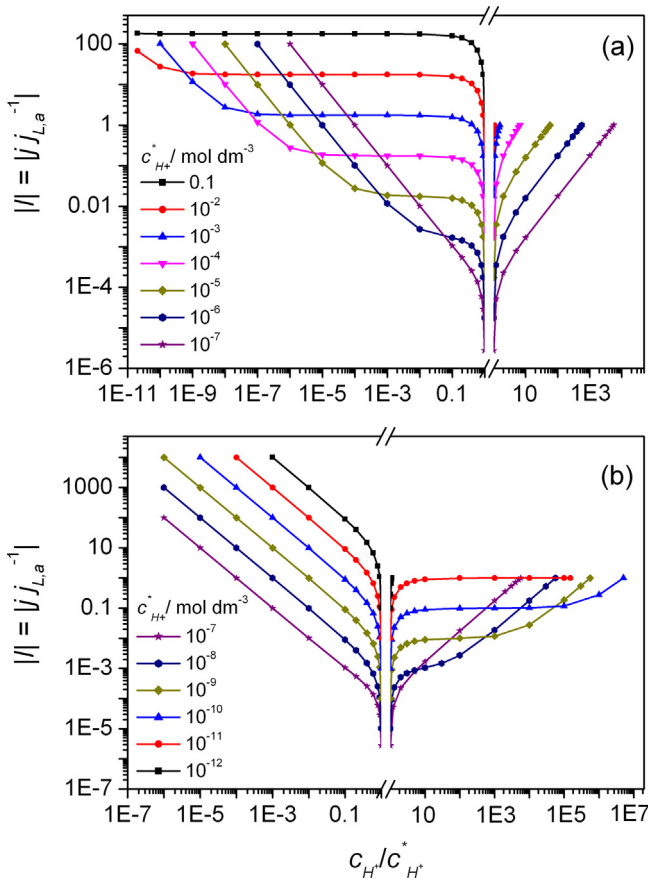
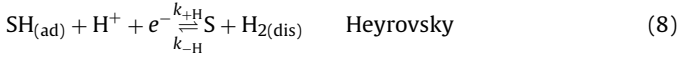
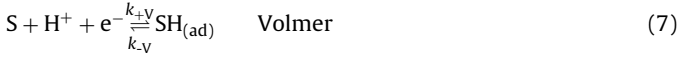


Fig. 1. Dependence of the normalized current density on the normalized surface concentration of protons in acid (a) and alkaline (b) solutions, simulated with Eq. (4) for different values of $c_{H^+}^*$ indicated in the graphs.

2.2. Kinetic model

The mechanism of the HER involves the Volmer (V), Heyrovsky (H) and Tafel (T) elementary steps, that can be represented by Eqs. (7)–(9) [1,2], where S denotes an active site.



The HER reaction rate in steady state (ν) is related to the elementary reaction rates (ν_i , i: V, H, T) through Eq. (10) [2,5,23].

$$\frac{j}{F} = \nu = \nu_V + \nu_H = 2(\nu_V - \nu_T) \quad (10)$$

Besides, the dependences of these elementary reaction rates on the overpotential ($\eta = E - E_{eq}$, where E_{eq} is the HER equilibrium potential at $c_{H^+}^*$ and P_{H_2}) and on the kinetic parameters are given by Eqs. (11)–(13).

$$\nu_V = \nu_V^e \left[\frac{\theta}{\theta^e} e^{\alpha f \eta} - C_{H^+} \frac{(1-\theta)}{(1-\theta^e)} e^{-(1-\alpha)f \eta} \right] \quad (11)$$

$$\nu_H = \nu_H^e \left[C_{H_2} \frac{(1-\theta)}{(1-\theta^e)} e^{\alpha f \eta} - C_{H^+} \frac{\theta}{\theta^e} e^{-(1-\alpha)f \eta} \right] \quad (12)$$

$$\nu_T = \nu_T^e \left[C_{H_2} \frac{(1-\theta)^2}{(1-\theta^e)^2} - \frac{\theta^2}{\theta^e} \right] \quad (13)$$

In these equations, the elementary kinetic rate constants ($k_{\pm i}$, i: V, H, T) are involved into the elementary equilibrium reaction rates (ν_i^e) [24] and the activity coefficients of dissolved species were approximated to 1 ($a_{c,i} \approx c_i$). Besides, α is the symmetry factor (supposed equal for both electrochemical steps) and $f = F/RT$. The reaction rate was assumed to be positive for the oxidation direction. The behavior of $H_{(ad)}$ was modeled through a Langmuir isotherm, being θ and θ^e the coverage of $H_{(ad)}$ at η and at $\eta = 0$ (equilibrium potential), respectively. It should be remarked that a more complex model that takes into account the interaction between adsorbed species, such as the Frumkin (or Temkin) isotherm [1,25], should be more realistic. As this is particularly critical for modeling the HER when precise calculations of kinetic parameters are required [5], this surely should be an issue to improve in a refined version of the equations.

Taking into account the relationship between C_{H^+} and C_{H_2} given by Eq. (A5), and by substituting Eqs. (11)–(13) into Eq. (10), two independent $j(\eta)$ dependences given by Eqs. (14) and (15) can be obtained.

$$\frac{j}{j_{L,a}} = \frac{\nu_V^e e^{\alpha f \eta} \left[\frac{\theta}{\theta^e} - C_{H^+} \frac{(1-\theta)}{(1-\theta^e)} e^{-f \eta} \right] + \nu_H^e e^{\alpha f \eta} \left[\frac{(1-\theta)}{(1-\theta^e)} - C_{H^+} \frac{\theta}{\theta^e} e^{-f \eta} \right]}{\frac{j_{L,a}}{F} + \nu_H^e \frac{(1-\theta)}{(1-\theta^e)} e^{\alpha f \eta}} \quad (14)$$

$$\frac{j}{j_{L,a}} = \frac{\nu_V^e e^{\alpha f \eta} \left[\frac{\theta}{\theta^e} - C_{H^+} \frac{(1-\theta)}{(1-\theta^e)} e^{-f \eta} \right] - \nu_T^e \left[\left(\frac{1-\theta}{1-\theta^e} \right)^2 - \left(\frac{\theta}{\theta^e} \right)^2 \right]}{\frac{j_{L,a}}{2F} - \nu_T^e \left(\frac{1-\theta}{1-\theta^e} \right)^2} \quad (15)$$

These two equations, together with Eq. (4), establish the dependences of j , θ and c_{H^+} on η , and can be used to correlate the experimental $j(\eta)$ curves measured for the HER and to obtain from these correlations the involved mechanistic parameters.

The equilibrium rates are evaluated at the equilibrium potential, which depends on the dimensionless a_{c,H^+} and hydrogen fugacity (f_{H_2}) through the Nernst equation. Thus, the equilibrium rates depend on these two variables according to Eqs. (16)–(18) [24], where K_T is the equilibrium constant of the Tafel step ($K_T = k_{+T}/k_{-T}$), and θ^e is a function of f_{H_2} given by Eq. (19). Note that both a_{c,H^+} and f_{H_2} can be approximated by $c_{H^+}^*$ and P_{H_2} .

$$\nu_V^e = \frac{k_{+V} K_T^{1/2} (a_{c,H^+})^\alpha (f_{H_2})^{\frac{1-\alpha}{2}}}{K_T^{1/2} + f_{H_2}^{1/2}} \cong \frac{k_{+V} K_T^{1/2} (c_{H^+}^*)^\alpha (P_{H_2})^{\frac{1-\alpha}{2}}}{K_T^{1/2} + P_{H_2}^{1/2}} \quad (16)$$

$$\nu_H^e = \frac{k_{+H} (a_{c,H^+})^\alpha (f_{H_2})^{1-\frac{\alpha}{2}}}{K_T^{1/2} + f_{H_2}^{1/2}} \cong \frac{k_{+H} (c_{H^+}^*)^\alpha (P_{H_2})^{1-\frac{\alpha}{2}}}{K_T^{1/2} + P_{H_2}^{1/2}} \quad (17)$$

$$\nu_T^e = \frac{k_{+T} f_{H_2}}{(K_T^{1/2} + f_{H_2}^{1/2})^2} \cong \frac{k_{+T} P_{H_2}}{(K_T^{1/2} + P_{H_2}^{1/2})^2} \quad (18)$$

$$\theta^e = \frac{f_{H_2}^{1/2}}{K_T^{1/2} + f_{H_2}^{1/2}} \cong \frac{P_{H_2}^{1/2}}{K_T^{1/2} + P_{H_2}^{1/2}} \quad (19)$$

The polarization resistance at the equilibrium potential ($R_p = \partial \eta / \partial j|_{\eta=0}$) can be obtained from Eqs. (4), (14) and (15) as it is detailed in Appendix A. The resulting dependence of R_p on the kinetic and mass-transport parameters is given by Eq. (20).

$$R_p = R_p^0 + \frac{RT}{Fj_{L,a}} \left(\frac{1}{2} + \frac{1}{\xi(1+\psi)} \right) \quad (20)$$

The contributions of kinetics and mass transport are very well separated in this dependence. On the one hand, the parameter R_p^0 is the activated polarization resistance at equilibrium, which depends only on the kinetic rate constants of the elementary steps through Eq. (21) [24,26].

$$R_p^0 = \frac{RT}{4F^2} \left(\frac{\nu_V^e + \nu_H^e + 4\nu_T^e}{\nu_V^e \nu_H^e + \nu_V^e \nu_T^e + \nu_H^e \nu_T^e} \right) = \frac{RT}{4F^2 P_{H_2}^{(1-\alpha)/2}} \left\{ \frac{(K_T^{1/2} + P_{H_2}^{1/2}) \left[\frac{4k_{+T}}{c_{H^+}^{*\alpha}} + (K_T^{1/2} + P_{H_2}^{1/2}) P_{H_2}^{-1/2} (k_{+V} K_T^{1/2} + k_{+H} P_{H_2}^{1/2}) \right]}{(K_T^{1/2} + P_{H_2}^{1/2}) k_{+V} k_{+H} K_T^{1/2} c_{H^+}^{*\alpha} P_{H_2}^{-\alpha/2} + k_{+H} k_{+T} P_{H_2}^{1/2} + k_{+V} k_{+T} K_T^{1/2}} \right\} \quad (21)$$

On the other hand, the second term of Eq. (20) involves the effects of mass transport of dissolved H_2 and H^+ , and of the water dissociation reaction. In very acid solutions where $\psi \ll 1$ and ξ is very large, Eq. (20) reduces to the previously reported dependence of R_p on $j_{L,a}$ [26].

It should be noted that for extremely large elementary rates ($R_p^0 \rightarrow 0$), the dependences defined by Eqs. (14), (15), and (20) reduce to those corresponding to a diffusion-controlled reaction (j^{dif} and R_p^{dif}), given by Eqs. (22) and (23).

$$\frac{j^{dif}}{j_{L,a}} = 1 - e^{2f\eta} C_{H^+}^2 \quad (22)$$

$$R_p^{dif} = \frac{RT}{Fj_{L,a}} \left(\frac{1}{2} + \frac{1}{\xi(1+\psi)} \right) \quad (23)$$

Moreover, the exchange current density of the HER (j^0) can be calculated with the kinetic parameters from Eq. (24) [27].

$$j^0 = 2F \left(\frac{\nu_V^e \nu_H^e + \nu_V^e \nu_T^e + \nu_H^e \nu_T^e}{\nu_V^e + \nu_H^e + 2\nu_T^e} \right) = \frac{2F}{(K_T^{1/2} + 1)} \left[\frac{\frac{k_{+T}}{(K_T^{1/2} + 1)} \left(1 + \frac{k_{+H}}{k_{+V} K_T^{1/2}} \right) + k_{+H} c_{H^+}^{*\alpha}}{1 + \frac{k_{+H}}{k_{+V} K_T^{1/2}} + \frac{2k_{+T}}{k_{+V} K_T^{1/2} (K_T^{1/2} + 1) c_{H^+}^{*\alpha}}} \right] \quad (24)$$

3. Experimental

3.1. Electrodes

Platinum disk microelectrodes with radii (r) in the range $2\text{ }\mu\text{m} \leq r \leq 12.5\text{ }\mu\text{m}$ were fabricated by heat sealing of sharpened wires into borosilicate glass capillaries by a procedure previously used for fabrication of SECM Pt tips [28]. Platinum wires (25 μm diameter, Alpha Aesar) were electrochemically etched in solution of 4.5 M CaCl_2 in 1 M HCl, by applying an ac voltage (sine wave, 50 Hz, $\pm 2\text{ V}$ peak to peak) against a concentric annular Pt counter-electrode (5 mm opening). The etched wire with a sharp tip was then introduced into a borosilicate glass capillary (1 mm outer diameter, 0.1 mm thickness), which end was melted by careful heating under a torch flame until the sealing of about 2 mm of the etched wire was visually verified. The sealed capillary was polished with a sequence of sandpapers (down to 2500 grits) and with a polishing pad with alumina slurry until the exposure of the metal disk was detected. The quality and size of the microelectrodes were evaluated by optical microscopy and cyclic voltammetry in ferrocene methanol solutions [29].

3.2. Electrochemical experiments

The HER was studied in 0.2 M LiClO_4 solutions (Merck). The pH was changed by addition of 0.2 M HClO_4 (Merck) or NaOH (Merck) solutions. Water used in all solutions was first deionized with an

exchange resin, then doubly distilled, and finally treated with a Purelab purifier (Elga Labwater, resistivity $\geq 18.2\text{ M}\Omega\text{ cm}$). The pH of the solutions was measured after the electrochemical experiments using a glass electrode (calibrated with buffers of pH 10, 7,

4 or 1), and a pH meter. All electrochemical measurements were performed using a PC-commanded potentiostat CHI-1140B (CH Instruments). A three-electrode cell was used, where the Pt microelectrode was the working electrode and a large-area Pt wire placed in the same vessel was the counter-electrode. The reference electrode was a saturated calomel electrode (SCE) placed in a separate compartment filled with the same cell solution and connected to the cell through a Luggin capillary. Saturation of the solutions with gas (H_2 or N_2) was attained by bubbling the purified gases through a glass pipe with holes that allowed the circulation of the solution in intimate contact with the gas. Thus, the solution was quickly saturated with the bubbling gas while agitation of the bulk solution was negligibly. The open-circuit potentials of the microelectrodes in acid ($\text{pH} < 5$) and alkaline ($\text{pH} > 9$) H_2 -saturated solutions were measured against the SCE using a high-sensitivity voltmeter. These values were identical to those measured on a large platinum wire in the same solution. However, due to the high polarization resistances verified in near-neutral solutions ($5 \leq \text{pH} \leq 9$), the zero-current potentials were measured galvanostatically in these conditions. All the potentials measured over the whole pH range (from acid to alkaline) changed with the pH with a slope of approximately -0.059 V dec^{-1} which verifies that they corresponded to the HER equilibrium potentials. Thus, the values of η were calculated using these measured equilibrium potentials. Steady-state polarization curves for the HER were measured in solutions saturated with H_2 at 1 atm. The curves were acquired point by point, either over the complete potential range every 0.025 V, or around the equilibrium potential every 1 mV (for the determination of R_p). A potential program including oxidation ($\eta = 1.2\text{ V}$) and reduction ($\eta = 0.1\text{ V}$) steps before each measuring step was used [6,26]. The cleanliness of electrodes and solutions was checked by cyclic voltammetry in solutions saturated with N_2 at 1 atm just before the HER experiments [26]. The real areas of the Pt microelectrodes were estimated from these voltammograms using the charge of upd-H adsorption [30]. These values resulted slightly larger than the respective geometric areas calculated from the microelectrode sizes (roughness factors in the range 1.2–1.5), which is typical of mechanically polished Pt electrodes.

4. Results and discussion

4.1. Simulations

4.1.1. General considerations

The surface concentrations of H_2 , H^+ and HO^- at each potential are controlled by the HER reaction rate, the mass transport, and the water dissociation through Eqs. (4), (14) and (15). Therefore, simulations of the $j(\eta)$ dependences were performed using these equations with the goal to analyze the effects of these parameters on the features of the polarization curves. These calculations were carried out using the software Mathcad 2000 Professional (Mathsoft).

The independent kinetic parameters that are involved in these equations are k_{+V} , k_{+H} , k_{+T} and K_T . All the other kinetic constants can

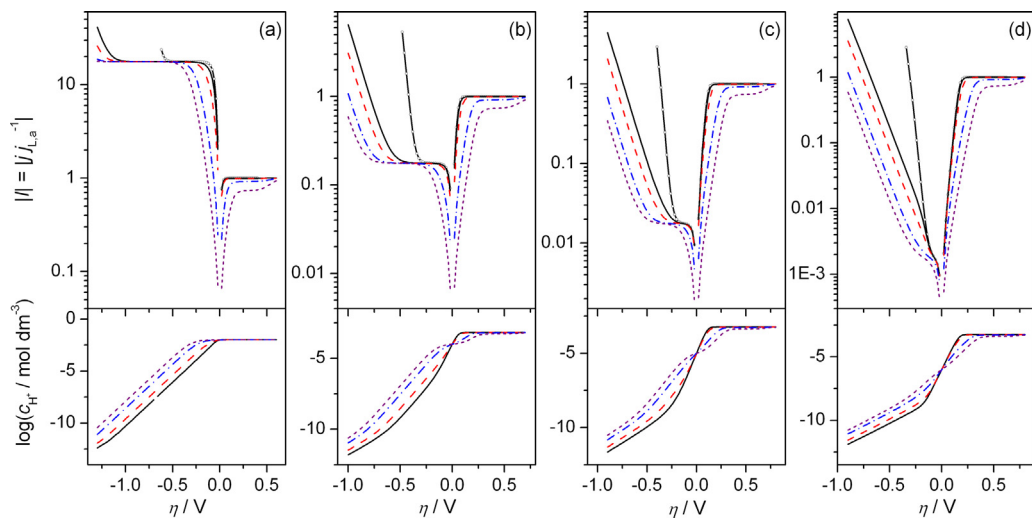


Fig. 2. Dependences of the normalized current density and of the surface concentration of protons on the overpotential in acid conditions, simulated using Eqs. (4), (14) and (15) for different mass-transport rates and with the following kinetic parameters: $k_{+V} = 7 \times 10^{-5}$; $k_{+H} = 2 \times 10^{-7}$; $k_{+T} = 1 \times 10^{-4}$; $K_T = 35$ (k_{+i} in $\text{mol s}^{-1} \text{cm}^{-2}$). $c_{\text{H}^+}^* (\text{mol dm}^{-3}) = 10^{-2}$ (a), 10^{-4} (b), 10^{-5} (c), 10^{-6} (d). $j_{L,a} (\text{A cm}^{-2}) = 0.001$ (solid lines), 0.005 (dashed lines), 0.05 (dot dashed lines), 0.2 (dotted lines). The diffusion controlled $I(\eta)$ dependences are also included (line + symbols).

be calculated from this set, and they constitute the only solution for each $j(\eta)$ dependence [24]. Thus, the magnitudes and relative values of these constants govern the behavior of the $j(\eta)$ curves and of the $\theta(\eta)$ and $c_{\text{H}^+}(\eta)$ dependences. This information is not available for most of the metals that are usually employed as electrodes for the HER. Even for Pt, the values of some of these parameters still are uncertain. In this context, the analysis of the descriptive capabilities of the reported equations is carried out in this work using kinetic constants with values in the order of those calculated from the different reported equilibrium rates for Pt [5,31].

This analysis makes the assumption that the solubility of H_2 and the diffusion coefficients of H^+ and $\text{H}_{2(\text{dis})}$ are independent of the solution pH. In fact, small changes in these values, and so in the values of ξ and ψ , could be expected as the pH changes [4–6,11]. On the other hand, not less important is the hypothesis that the nature of the electrode surface is invariant with the pH. This approximation is probably not real taking into account that the pH varies over such a wide range that the point of zero charge of any material will surely be crossed. However, as the goal of these simulations is to

explore the main descriptive capabilities of the presented model, these changes are not considered in the present analysis.

4.1.2. Effects of the mass-transport rate and pH

The simulated dependences of $j(\eta)$ normalized respect to $j_{L,a}$ ($I = j(\eta)/j_{L,a}$) as a function of η for different $j_{L,a}$ values are plotted in Figs. 2 and 3 for various values of $c_{\text{H}^+}^*$ in acid and alkaline solutions, respectively. These plots illustrate the effects of mass transport rate on the $I(\eta)$ responses at different pH values for these kinetic parameters. In trying to make a parallel with real conditions, it should be pointed out that an RDE can reach, as a maximum, the situation given by the dashed lines ($j_{L,a} < 5 \text{ mA cm}^{-2}$). Larger $j_{L,a}$ values can be reached using microelectrodes with dimensions in the range comprised between $10 \mu\text{m}$ and 10 nm . The $I(\eta)$ curves that correspond to a reversible (or diffusion controlled) reaction indicate the fastest limiting situation. These diffusion-controlled curves indicate the values of $j_{L,a}$ that are required to separate the $I(\eta)$ response from a pure diffusion control, for the selected kinetic parameters. These simulations show that the deviation of the $I(\eta)$ curves from

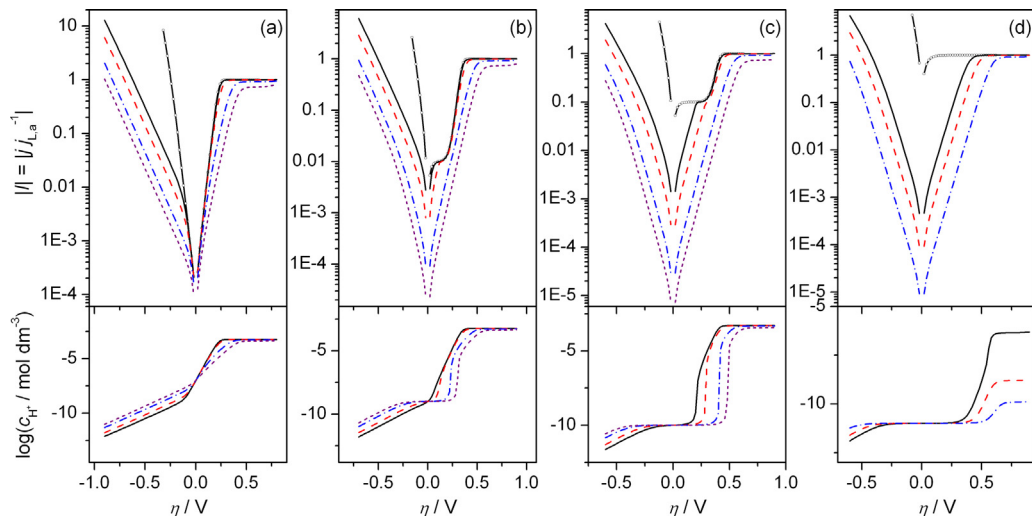


Fig. 3. Dependences of the normalized current density and of the surface concentration of protons on the overpotential in neutral and alkaline conditions, simulated using Eqs. (4), (14) and (15) for mass-transport and kinetic parameters as those of Fig. 2. $c_{\text{H}^+}^* (\text{mol dm}^{-3}) = 10^{-7}$ (a), 10^{-9} (b), 10^{-10} (c), 10^{-11} (d).

a mass-transport controlled dependence is strongly dependent on the pH and on the potential range.

In acid solutions (Fig. 2) the *hor* always should reach a constant current due to diffusion of H^+ (j_{H^+}) over a potential range that depends on the pH and on the kinetic parameters. As the value of j_{H^+} is in fact proportional to $c_{H^+}^*$ through Eq. (5), in very acid solutions the j_{H^+} values are very large. Then, the formation of H_2 bubbles is verified at η values where j_{H^+} still is not reached, and thus j_{H^+} is not experimentally observed in strongly acid conditions. At more cathodic overpotentials where the surface concentration of protons drops below 10^{-7} M, protons coming from water dissociation start to be reduced and a new increase of the current is verified (so-called water discharge). A strong effect of mass transport conditions on the water discharge is verified. Besides, in the more acid solutions the onset potential for the water discharge for these kinetic parameters is significantly separated from that expected for a diffusion-controlled response, although they approach as the pH increases. Moreover, the extension of the potential range where j_{H^+} is established becomes narrower as the pH increases.

On the other hand, in these slightly acid conditions the behavior of the *hor* is similar to that verified in strongly acid solutions [6,31,32]. More precisely, at low overpotentials ($\eta < 0.2$ V) the *hor* reaches a maximum current density (j_{max}) that has kinetic and mass-transport contributions [23], and which value is very close

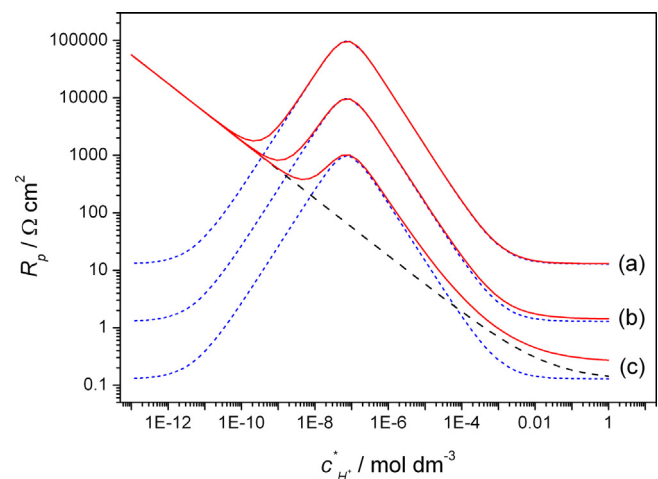


Fig. 4. Simulated dependences of R_p (solid lines), R_p^0 (dashed line) and R_p^{diff} (dotted lines) on $c_{H^+}^*$ for the kinetic parameters indicated in Fig. 2 and different mass-transport rates $j_{L,a}$ ($A\text{cm}^{-2}$) = 0.001 (a), 0.01 (b), 0.1 (c).

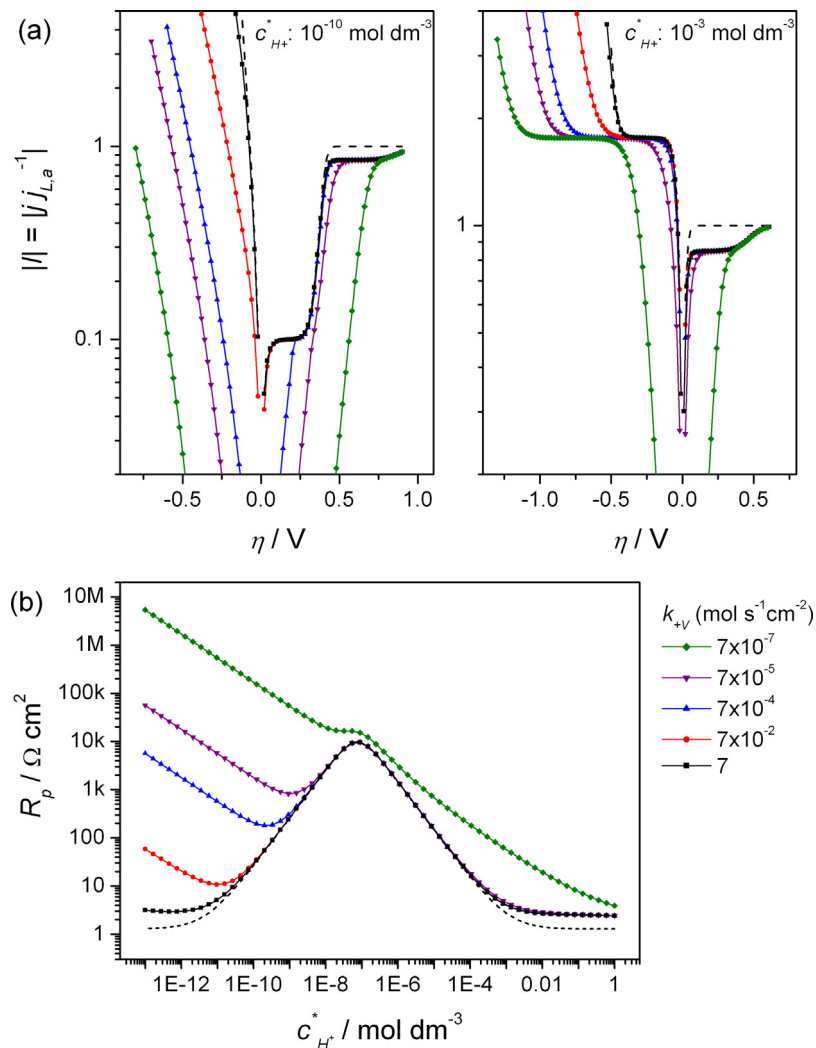


Fig. 5. Effect of k_{+V} in the $I(\eta)$ (a) and $R_p(c_{H^+}^*)$ (b) dependences. $j_{L,a} = 0.01\text{ A cm}^{-2}$. Fixed kinetic parameters: $k_{+H} = 2 \times 10^{-7}$; $k_{+T} = 1 \times 10^{-5}$; $K_T = 35$ (k_{+i} in $\text{mol s}^{-1} \text{cm}^{-2}$). The diffusion-controlled dependences are also included (dashed lines).

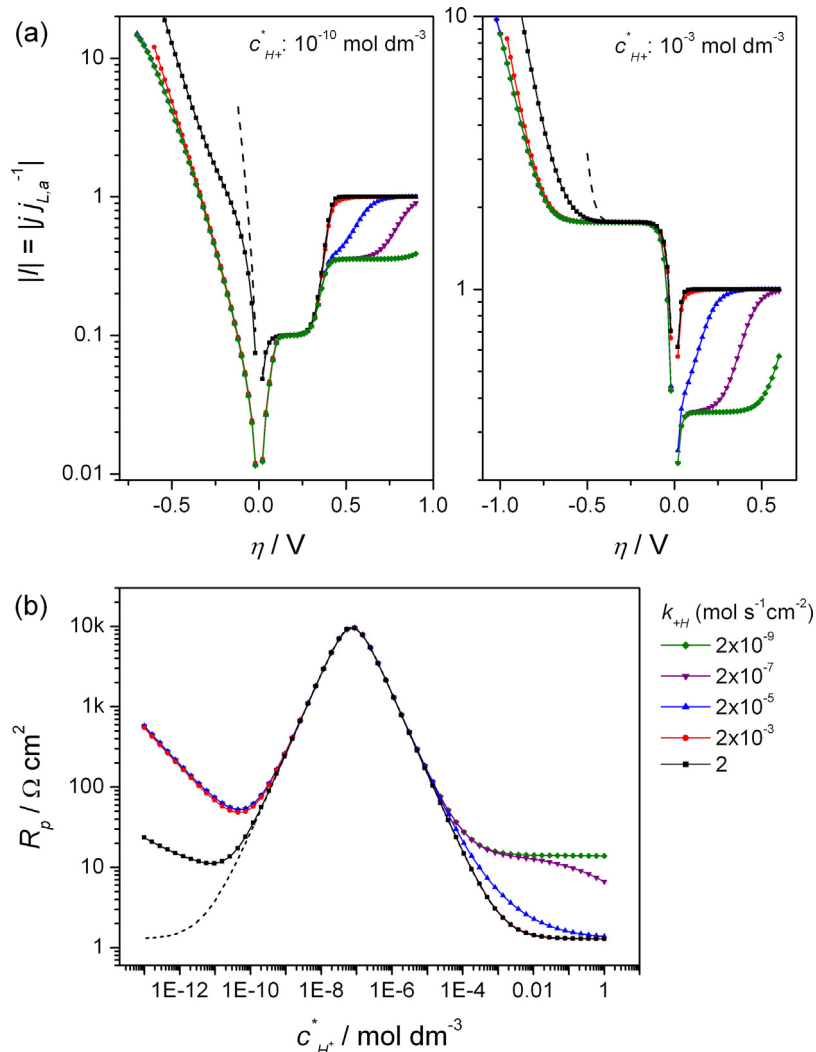


Fig. 6. Effect of k_{+H} in the $I(\eta)$ (a) and $R_p(c_{H+}^*)$ (b) dependences. $j_{L,a} = 0.01 \text{ A cm}^{-2}$. Fixed kinetic parameters: $k_{+V} = 7 \times 10^{-3}$; $k_{+T} = 1 \times 10^{-6}$; $K_T = 35$ (k_{+i} in $\text{mol s}^{-1} \text{cm}^{-2}$). The diffusion-controlled dependences are also included (dashed lines).

to $j_{L,a}$ when the mass transport rate is low. The values of j_{max} and $j_{L,a}$ can be clearly differentiated when the ratio $j_{max}/j_{L,a}$ becomes smaller than 0.95, which occurs when $j_{L,a} > 5 \text{ mA cm}^{-2}$ for these kinetic parameters. At higher η values the *hor* current restart increasing due to the Heyrovsky step, which becomes important at large η values [31].

In neutral and alkaline solutions (Fig. 3) the *her* proceeds using water as the main source of H^+ , and thus the current increases continuously for more negative η values. In spite of being water the main reactant, in neutral media the mass transport conditions still produce some effects on the $I(\eta)$ responses for these kinetic parameters. The reaction becomes slower in alkaline solutions since the equilibrium rates of Volmer and Heyrovsky steps decrease as c_{H+}^* becomes smaller through Eqs. (16) and (17). Thus, the $j(\eta)$ dependences in alkaline media separate markedly from the reversible curves in all the analyzed mass-transport conditions. As in the acid media, the *hor* current density approaches to j_{max} at low η values, and eventually tends to $j_{L,a}$ at very large η values. Moreover, over the concentration range $10^{-8} < c_{H+}^* (\text{mol dm}^{-3}) < 10^{-11}$, as it was previously indicated, the *hor* verifies the presence of a constant current density caused by the diffusion of $\text{HO}^- (j_{\text{HO}^-})$. The value of j_{HO^-} is, in general, smaller than j_{max} . However, under conditions of very large $j_{L,a}$ values, j_{max} may decrease below the j_{HO^-} value.

It is interesting to analyze the $I(\eta, c_{H+}^*)$ dependences that result from the simulations in near neutral solutions around the equilibrium potential ($-0.1 \text{ V} < \eta < 0.1 \text{ V}$). In these conditions, the $I(\eta)$ dependences approach considerably to the corresponding $I^{dif}(\eta)$ curves. This observation can be better appreciated in Fig. 4, that shows the dependency of R_p on c_{H+}^* simulated with Eq. (20) for different mass-transport conditions. These $R_p(c_{H+}^*)$ dependences are contrasted against the respective $R_p^0(c_{H+}^*)$ and $R_p^{dif}(c_{H+}^*, j_{L,a})$ functions. In solutions with low pH values, R_p clearly separates from R_p^{dif} , being this difference larger as $j_{L,a}$ increases. The separation between R_p and R_p^{dif} becomes larger for increasing pH values, since R_p^0 grows faster than R_p^{dif} when c_{H+}^* decreases. However, for pH values larger than 2, R_p^{dif} becomes more sensitive to c_{H+}^* and its value starts increasing faster than R_p^0 as c_{H+}^* decreases. Besides, the $R_p^{dif}(c_{H+}^*)$ dependence reaches a maximum for $c_{H+}^* \cong 10^{-7} \text{ M}$, and then decreases at smaller values of c_{H+}^* . Thus, the contribution of R_p^{dif} to R_p becomes more important in the range $10^{-8} \leq c_{H+}^* (\text{mol dm}^{-3}) \leq 10^{-3}$, especially in conditions of low $j_{L,a}$ values. Only in conditions of very large $j_{L,a}$ values ($> 0.1 \text{ A cm}^{-2}$) the value of R_p separates from the R_p^{dif} in this pH range. Contrarily, in alkaline

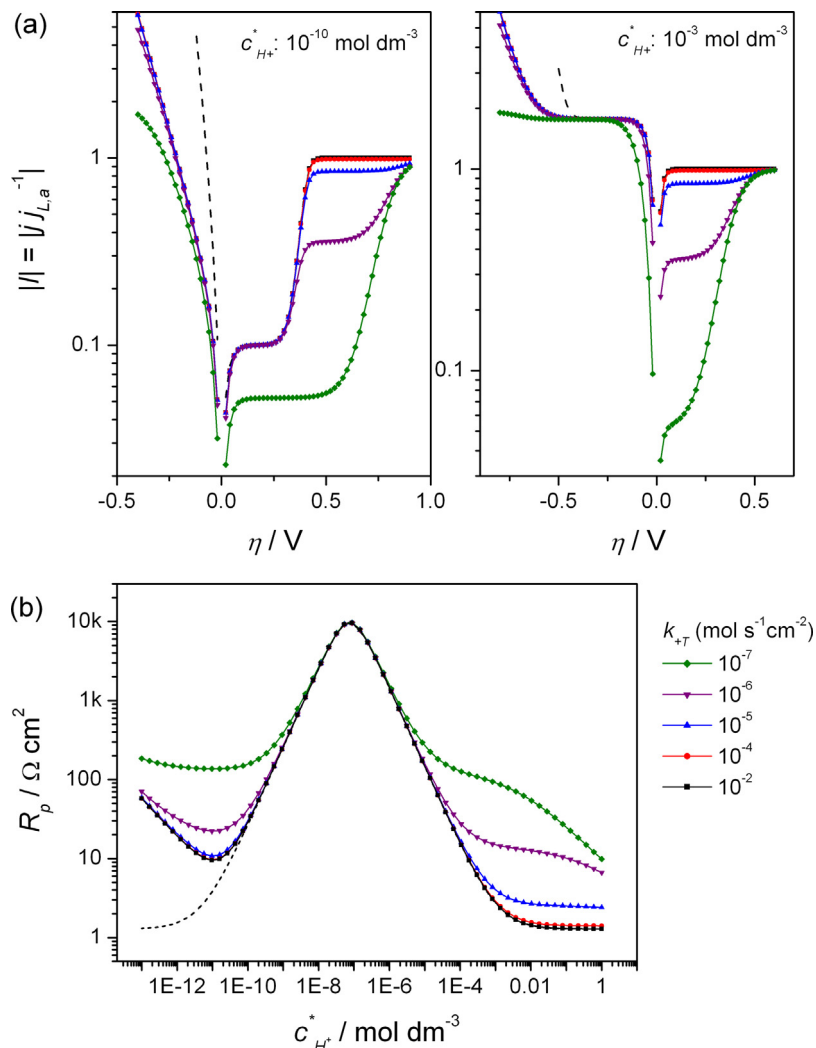


Fig. 7. Effect of k_{+T} in the $I(\eta)$ (a) and $R_p(c_{H^+}^*)$ (b) dependences. $j_{La} = 0.01 \text{ A cm}^{-2}$. Fixed kinetic parameters: $k_{+V} = 7 \times 10^{-2}$; $k_{+H} = 2 \times 10^{-7}$; $K_T = 35$ (k_{+i} in $\text{mol s}^{-1} \text{cm}^{-2}$). The diffusion-controlled dependences are also included (dashed lines).

solutions as R_p^{dif} decreases and R_p^0 keeps growing for decreasing $c_{H^+}^*$ values, R_p becomes almost purely kinetically controlled ($R_p \cong R_p^0$) independently of the j_{La} value.

4.1.3. Effect of kinetic parameters

The effect of k_{+V} is observed in Fig. 5, which shows simulations of $I(\eta)$ curves (Fig. 5a) for two representative pH values, and of $R_p(c_{H^+}^*)$ curves (Fig. 5b). For these conditions, a decrease of k_{+V} produces a shift of the *her* $I(\eta)$ curves toward more negative η values. This shift is much more prominent in conditions where water acts as the main source of protons. Thus, while k_{+V} governs the whole *her* $I(\eta)$ curve in alkaline solutions, its effect on the *her* in acid solutions is more evident at large η values where water discharge takes place. Besides, with water as reactant the *her* would operate under pure diffusion control only for very large k_{+V} values (>5). Thus, it can be concluded that the analysis of the *her* curves in conditions where water is the reactant should provide very accurate values of k_{+V} , since the curves in these conditions are very sensitive to this parameter. On the other hand, the same shift of the *hor* $I(\eta)$ curves is observed upon decreasing k_{+V} , although much smaller values are required to clearly separate from the diffusion controlled curve at low η values. As can be seen in Fig. 5b, the polarization resistance is strongly affected by the value of k_{+V} in alkaline media, while little

effect of this parameter is verified in acid and neutral media, unless it is very small ($<10^{-5}$).

The effect of k_{+H} is illustrated in the simulations shown in Fig. 6. The main effect of k_{+H} on the $I(\eta)$ curves is observed on the *hor*. When $k_{+H} \ll k_{+T}$, the normalized kinetic limiting current ($I_{max} = j_{max}/j_{La} < 1$) is established over a range of η that becomes narrower as the k_{+H} value grows and approaches k_{+T} . When k_{+H} is in the order of k_{+T} , just a shoulder in the $I(\eta)$ curve is observed, which signals the transition between routes. When $k_{+H} \gg k_{+T}$ the current tends to the diffusion controlled value. On the other hand, particularly striking is the poor sensitivity of the *her* to the k_{+H} value, since this parameter only shows an appreciable effect on the water discharge when its value is very large. Finally, the effect of k_{+H} on R_p is only significant when the value of k_{+H} is in the order or larger than k_{+T} in acid media, or many orders of magnitude larger than k_{+T} in alkaline media.

The value of k_{+T} has a more important effect on the *hor* part of the $I(\eta)$ curve (Fig. 7a), since this parameter governs the value of I_{max} . When k_{+T} grows to very large values, I_{max} approaches to 1 (j_{max} tends to j_{La}). On the contrary, when k_{+T} decreases the I_{max} value goes down and may become even smaller than I_{HO^-} in slightly alkaline solutions. On the other hand, under the analyzed conditions the *her* is much less sensitive to the value of k_{+T} . A clear effect is only observed when k_{+T} is in the order or smaller than

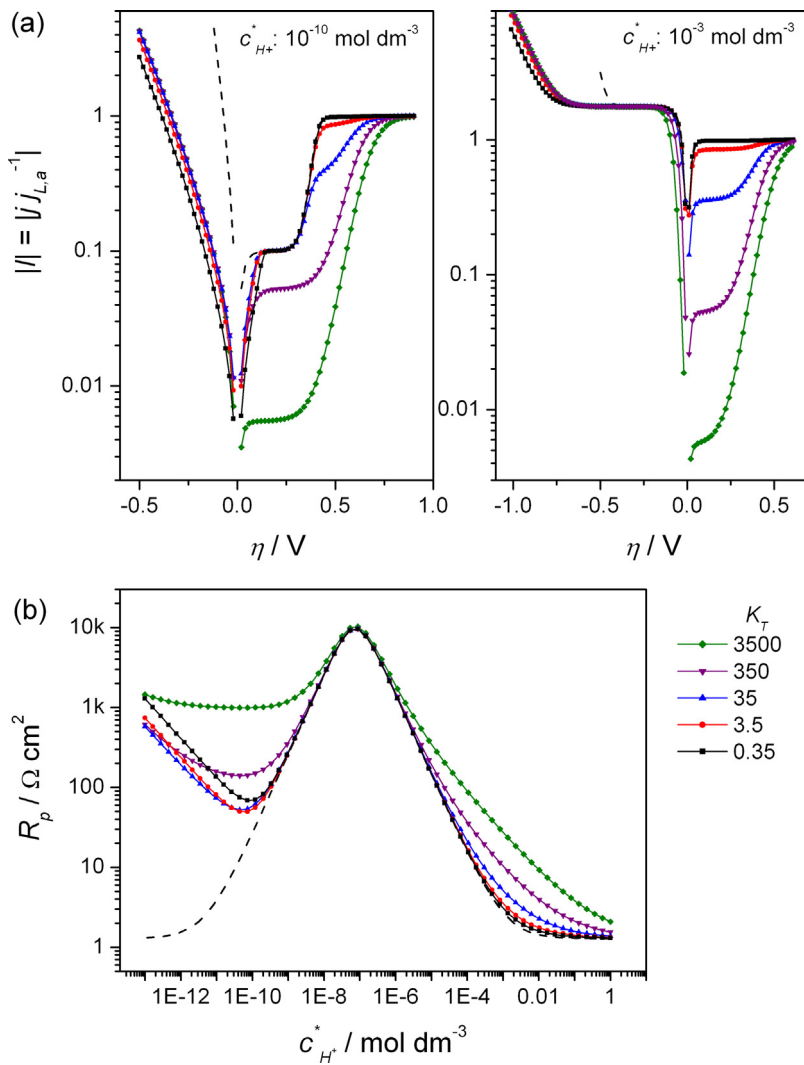


Fig. 8. Effect of K_T in the $I(\eta)$ (a) and $R_p(c_{H+}^*)$ (b) dependences. $j_{L,a} = 0.01 \text{ A cm}^{-2}$. Fixed kinetic parameters: $k_{+V} = 7 \times 10^{-3}$; $k_{+H} = 2 \times 10^{-5}$; $k_{+T} = 1 \times 10^{-6}$ (k_{+i} in $\text{mol s}^{-1} \text{ cm}^{-2}$). The diffusion-controlled dependences are also included (dashed lines).

k_{+H} . Moreover, Fig. 7b shows that R_p is strongly affected by the k_{+T} value in acid solutions, but it is poorly sensitive to this parameter in alkaline media.

The value of K_T , which fix the equilibrium coverage of $H_{(ad)}$ through Eq. (19), produces significant effects on the *hor* part of the $I(\eta)$ curve (Fig. 8a), and particularly on I_{max} . In general, increasing values of K_T (smaller θ^e values) lead to smaller I_{max} values. The *her* is much less affected by K_T for these kinetic parameters, and only a slight shift of the curves toward more negative η values are observed upon increasing K_T . On the other hand, Fig. 8b shows that the $R_p(c_{H+}^*)$ dependence is very sensitive to the K_T both in acid (where R_p grows for increasing K_T values) and in alkaline media.

4.2. Analysis of the HER on Pt microelectrodes

As it was indicated previously, steady-state $I(\eta)$ curves for the HER were measured on Pt disk microelectrodes in solutions with different pH values. A complete set of curves measured on a Pt microelectrode (radius = 4.5 μm) is shown in Fig. 9 (acid solutions) and Fig. 10 (alkaline solutions). These experimental curves show the features previously described related to the mass transport and the water dissociation reaction, as well as the kinetic characteristics. Thus for example, the constant currents due to diffusion of H^+ (I_{H^+}) and HO^- (I_{HO^-}) are detected in slightly acid and alkaline solutions, respectively. These values are in accordance with

Table 1

Kinetic parameters used to simulate the theoretical $I(\eta)$ dependences shown in Figs. 9 and 10 (k_{+i} in $\text{mol s}^{-1} \text{ cm}^{-2}$) and exchange current densities calculated from Eq. (24).

pH	k_{+V}	k_{+H}	k_{+T}	K_T	j^0 (A cm^{-2})
2.9	3.66×10^{-3}	0.82×10^{-5}	8.36×10^{-4}	2×10^3	0.078
3.6	1.91×10^{-3}	0.99×10^{-5}	7.1×10^{-4}	1.5×10^3	0.085
4.7	2.22×10^{-3}	1.03×10^{-5}	3.75×10^{-4}	2.4×10^3	0.028
5.8	0.92×10^{-3}	1.75×10^{-5}	2.54×10^{-4}	1.2×10^3	0.029
7.5	2.09×10^{-3}	1.70×10^{-5}	7.72×10^{-4}	0.8×10^3	0.029
8.5	2.64×10^{-3}	2.4×10^{-5}	9.6×10^{-4}	1.0×10^3	0.0013
10.8	2.75×10^{-3}	8.1×10^{-5}	8.9×10^{-4}	1.1×10^3	0.00102
11.0	7.88×10^{-3}	9.7×10^{-5}	6.5×10^{-4}	0.76×10^3	0.00228

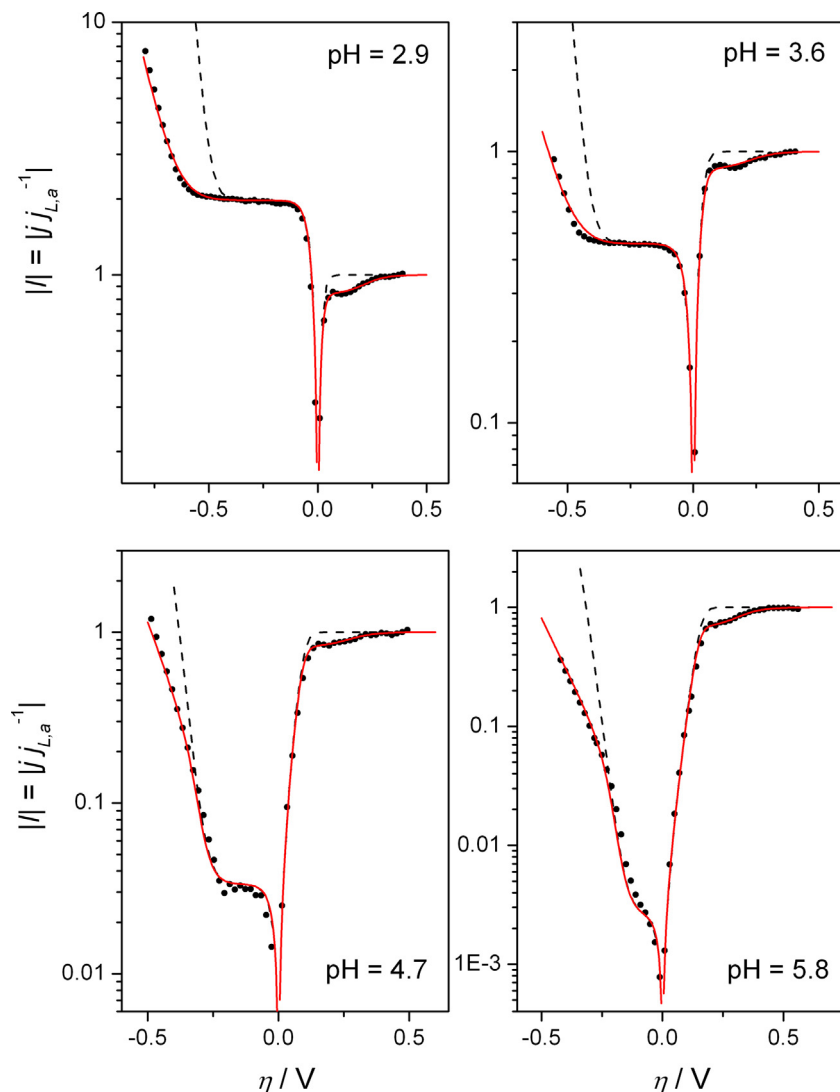


Fig. 9. Experimental $I(\eta)$ dependences (symbols) measured on a Pt disk microelectrode (radius = 4.5 μm , $j_{La} = 0.014 \pm 0.001 \text{ A cm}^{-2}$) in acid solutions (0.2 M ClO_4^-) and theoretical dependences (solid lines) simulated using kinetic parameters shown in Table 1. The diffusion-controlled dependences are also included (dashed lines).

the pH value measured with a glass electrode. Moreover, the current increment due to water discharge is observed to shift toward less negative overpotentials when the solution pH increases, and becomes the main reaction in neutral and alkaline solutions. It is also possible to observe the main kinetic aspects of the reaction, both in the *hor* (existence of a kinetically controlled limiting current) and in the *her* (a shifting of the onset potential for water discharge respect to the diffusion controlled curve). The effects of mass-transport rate on these features can be clearly seen in Fig. 11, which shows $I(\eta)$ curves measured on Pt microelectrodes with different sizes.

From a first qualitative analysis of plots shown in Figs. 9 and 10, it is clear that the reaction rate decreases as the pH increases. In general, the $I(\eta)$ curves at high overpotentials clearly separate from the reversible responses (dashed lines) in the *hor* at any pH and in the water discharge. However, in near neutral conditions at low overpotentials the differences between the experimental data and the reversible curve are very small. This fact is better appreciated in Fig. 12, that shows the experimental values of R_p plotted against $c_{\text{H}^+}^*$. Under the analyzed mass-transport conditions the experimental values of R_p separate in a detectable amount from the corresponding R_p^{dif} in acid solutions ($c_{\text{H}^+}^* > 10^{-3} \text{ M}$). The

measured R_p values are also much larger than R_p^{dif} in alkaline solutions ($c_{\text{H}^+}^* < 10^{-9} \text{ M}$). However, in the range $10^{-9} < c_{\text{H}^+}^* (\text{mol dm}^{-3}) < 10^{-3}$ the values of R_p^{dif} are so large that reliable experimental R_p values should hardly be measured. Thus, R_p values measured over this pH range are probably meaningless for kinetic analysis.

In order to contrast the present model with the experimental $I(\eta)$ curves and to make an estimation of the kinetic parameters, Eqs. (4), (14) and (15) were used to simulate theoretical dependences that approach reasonably well to the experimental data. Thus, the kinetic parameters were systematically varied, one at a time, until a combination that reproduced the whole analyzed curve was located. These theoretical curves are shown in Fig. 9 as solid lines, and the resulting kinetic parameters (rate constants and their respective pH-dependent exchange current densities) are presented in Table 1. It can be verified that for most of the studied pH values the developed model has the capability to describe the $I(\eta)$ dependences over the complete domain of analyzed overpotentials. The sets of kinetic constants that result from each independent analysis are reasonably similar. Probably the most remarkable aspect that is evidenced from this analysis

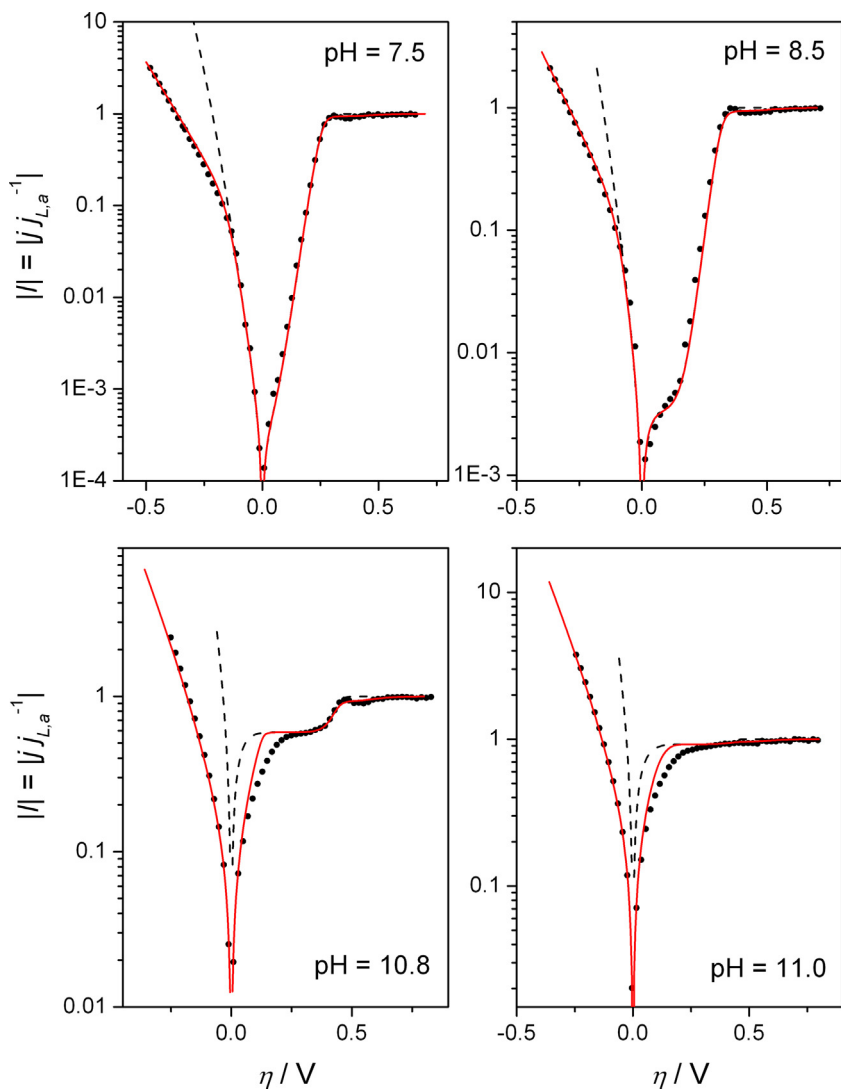


Fig. 10. Experimental $I(\eta)$ dependences (symbols) measured on a Pt disk microelectrode (radius = 4.5 μm , $j_{L,a} = 0.014 \pm 0.001 \text{ A cm}^{-2}$) in alkaline solutions (0.2 M ClO_4^-) and theoretical dependences (solid lines) simulated using kinetic parameters shown in Table 1. The diffusion-controlled dependences are also included (dashed lines).

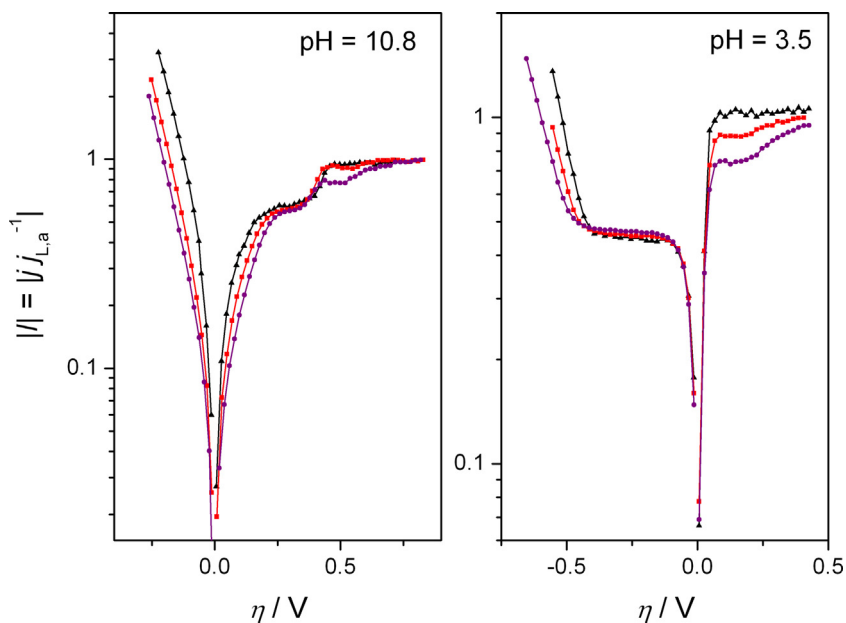


Fig. 11. Experimental $I(\eta)$ dependences measured on Pt disk microelectrodes with different sizes in alkaline and acid solutions (0.2 M ClO_4^-). Disk radius (μm)/ $j_{L,a}$ (A cm^{-2}): 12.5/0.005 (triangles), 4.5/0.014 (squares), 2.1/0.031 (circles).

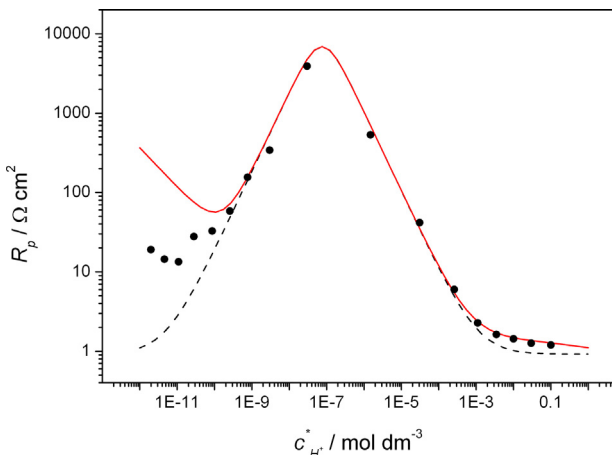


Fig. 12. Dependence of R_p on $c^*_{\text{H}^+}$ measured on a Pt disk microelectrode (radius = 4.5 μm , $j_{\text{L,a}} = 0.014 \pm 0.001 \text{ A cm}^{-2}$) in 0.2 M ClO_4^- solutions (symbols), and theoretical dependence (solid lines) simulated using mean values of the kinetic parameters shown in Table 1. $k_{\text{v}} = 3 \times 10^{-3}$; $k_{\text{H}} = 3.3 \times 10^{-5}$; $k_{\text{T}} = 6.8 \times 10^{-4}$; $K_{\text{T}} = 1300$ ($k_{\text{r},i}$ in $\text{mol s}^{-1} \text{cm}^{-2}$). The diffusion-controlled dependence is also included (dashed line).

is the high value of k_{v} required to properly describe the $I(\eta)$ dependence for water discharge. Not less important is the strong sensitivity of the *hor* to the value of k_{T} relative to k_{H} and $j_{\text{L,a}}$. The values of j^0 that were calculated with these kinetic constants and Eq. (24), are shown in Table 1. These values are in the order of those previously reported for polycrystalline Pt measured in conditions of high mass-transport rates [6], and vary from around 80 mA cm^{-2} in acid to near 1 mA cm^{-2} in alkaline media [9].

Notwithstanding, the equation is unable to reproduce part of the $I(\eta)$ curves measured in the alkaline solutions. On that sense, the *hor* part at low overpotentials cannot be followed by the model unless very different kinetic parameters are used. Similarly, the values of R_p measured in alkaline media are much smaller than those expected for the kinetic constants measured from $I(\eta)$ curves (solid line in Fig. 12). The reasons for this discrepancy between experimental and simulated data should be analyzed more deeply. It could be possible that a real change of the electrode behavior occurs in these conditions, or that fouling of the electrode by traces of contaminants becomes more important under these conditions. However, it could also be possible that the discrepancy is caused by an oversimplification in the model that becomes relevant in alkaline conditions (i.e. the adsorption model, or the kinetics of the water dissociation reaction).

5. Conclusions

The model developed in this work for the analysis of the HER in steady state describes the $I(\eta)$ and the $R_p(c^*_{\text{H}^+})$ dependences over a complete range of pH, including neutral, slightly acid and slightly alkaline media. This model is based on the description of the HER through the Volmer–Heyrovsky–Tafel mechanism, using H^+ as reactant (*her*) or product (*hor*), and including the water dissociation equilibrium. It was demonstrated that these dependences are particularly sensitive to some kinetic parameters of the HER over different domains of pHs and overpotentials. For example, a strong dependency of the water discharge with the kinetic constant of the Volmer step was verified. Besides, as the *hor* is strongly affected by the relative values of the Tafel and Heyrovsky parameters, this part of the curve can be used for precise calculation of these parameters. Moreover, the analysis of the $R_p(c^*_{\text{H}^+})$ dependency only is useful

in acid ($c^*_{\text{H}^+} > 10^{-3} \text{ mol dm}^{-3}$) or alkaline ($c^*_{\text{H}^+} < 10^{-10} \text{ mol dm}^{-3}$) solutions, since in near-neutral conditions the experimental values of R_p should approach very much to the diffusion controlled values even for very high mass-transport rates.

The developed equations describe satisfactorily the experimental $I(\eta)$ dependencies measured on Pt microelectrodes in neutral and acid media over both the cathodic (*her*) and anodic (*hor*) branches, and they were used to estimate the kinetic constants. Furthermore, the variations of the $I(\eta)$ curves and of the R_p values on pH are self consistent, as they can be described basically with the same set of kinetic parameters at any pH. However, in alkaline solutions the model is not able to reproduce part of the experimental $I(\eta)$ results with the same kinetic parameters. Besides, in this range of pH the $R_p(c^*_{\text{H}^+})$ dependence is only reproduced with other kinetic parameters. In view of this, it is necessary to carry out a more detailed analysis of the causes of this deviation to make appropriate modifications that render applicable the model on data measured in this pH range.

Acknowledgements

This work was supported by Agencia Nacional de Promoción Científica y Tecnológica (ANPCyT), Consejo Nacional de Investigaciones Científicas y Técnicas (CONICET) and Universidad Nacional del Litoral. The authors are very grateful to A.C. Chialvo for his comments and suggestions about this work.

Appendix A.

This appendix gives details on the derivation of Eqs. (4) and (20).

A.1. Derivation of Eq. (4)

From a mass balance at the electrode surface the relationship between the rate of the HER (v) and the concentration gradients of H^+ , HO^- and H_2 given by Eq. (A1) is verified, where D_i and c_i are diffusion coefficients and surface concentrations, respectively.

$$v = D_{\text{H}^+} \nabla c_{\text{H}^+} - D_{\text{HO}^-} \nabla c_{\text{HO}^-} = -2D_{\text{H}_2} \nabla c_{\text{H}_2} \quad (\text{A1})$$

As the reaction (3) is considered at equilibrium, the relationship between the concentration gradients of H^+ and HO^- results in Eq. (A2), where K_w is the equilibrium constant of reaction (3). When this is substituted in Eq. (A1) it leads to Eq. (A3).

$$\nabla c_{\text{HO}^-} = -\frac{K_w}{c_{\text{H}^+}^2} \nabla c_{\text{H}^+} \quad (\text{A2})$$

$$v = D_{\text{H}^+} \nabla c_{\text{H}^+} \left[1 + \left(\frac{D_{\text{HO}^-}}{D_{\text{H}^+}} \right) \frac{K_w}{c_{\text{H}^+}^2} \right] = -2D_{\text{H}_2} \nabla c_{\text{H}_2} \quad (\text{A3})$$

The second equality of Eq. (A3) relates the concentrations of H^+ and H_2 at the surface, which, taking into account the boundary condition given by Eq. (A4), leads to Eq. (A5). The normalized surface concentrations (c_i) are defined by $C_i = c_i/c_i^*$.

$$v = 0 : \quad c_{\text{H}^+} = c_{\text{H}^+}^* ; \quad c_{\text{H}_2} = c_{\text{H}_2}^* \quad (\text{A4})$$

$$C_{\text{H}_2} = 1 + \left(\frac{D_{\text{H}^+} c_{\text{H}^+}^*}{2D_{\text{H}_2} c_{\text{H}_2}^*} \right) \left[(1 - C_{\text{H}^+}) + \left(\frac{D_{\text{HO}^-} K_w}{D_{\text{H}^+} (c_{\text{H}^+}^*)^2} \right) \left(\frac{1}{C_{\text{H}^+}} - 1 \right) \right] \quad (\text{A5})$$

Taking into account that the H_2 concentration gradient can be written in terms of the diffusion layer thickness (δ), the current density of the HER ($j = Fv$) results from Eq. (A3) and Eq. (A5) in Eq.

(A6), which leads to Eq. (4).

$$j = \frac{2FD_{H_2}C_{H_2}^*}{\delta}(1 - C_{H_2}) = -\frac{FD_{H^+}C_{H^+}^*}{\delta} \times \left[(1 - C_{H^+}) + \left(\frac{D_{HO^-}K_w}{D_{H^+}(C_{H^+}^*)^2} \right) \left(\frac{1}{C_{H^+}} - 1 \right) \right] \quad (A6)$$

A.2. Derivation of Eq. (20)

The polarization resistance at the equilibrium potential ($R_p = \partial\eta/\partial j|_{\eta=0}$) can be obtained by taking the derivatives of Eqs. (4), (14) and (15) and evaluating them at $\eta=0$. This results in Eqs. (A7)–(A9), which can be combined to obtain Eq. (20).

$$\frac{\partial j}{\partial\eta} \Big|_{\eta=0} = \xi(1 + \psi)j_{L,a} \frac{\partial C_{H^+}}{\partial\eta} \Big|_{\eta=0} \quad (A7)$$

$$\frac{\partial j}{\partial\eta} \Big|_{\eta=0} = \frac{2F \left[i_V^e \left(\frac{\partial C_{H^+}}{\partial\eta} \right)_{\eta=0} - f \right] - (v_V^e + 2v_T^e) \left(\frac{1}{1-\theta^e} + \frac{1}{\theta^e} \right) \frac{\partial\theta}{\partial\eta} \Big|_{\eta=0}}{1 + \frac{2F}{j_{L,a}} i_T^e} \quad (A8)$$

$$\frac{\partial j}{\partial\eta} \Big|_{\eta=0} = \frac{2F \left[i_H^e \left(\frac{\partial C_{H^+}}{\partial\eta} \right)_{\eta=0} - f \right] + (v_H^e + 2v_T^e) \left(\frac{1}{1-\theta^e} + \frac{1}{\theta^e} \right) \frac{\partial\theta}{\partial\eta} \Big|_{\eta=0}}{1 - \frac{2F}{j_{L,a}} (v_H^e + v_T^e)} \quad (A9)$$

References

- [1] M. Enyo, Hydrogen electrode reaction on electrocatalytically active metals, in: B.E. Conway, J.O'M. Bockris, E. Yeager, S.U.M. Khan, R.E. White (Eds.), Comprehensive Treatise of Electrochemistry, vol. 7, Plenum Press, New York, 1983, p. 241 (Ch. 5).
- [2] M.R. Gennero de Chialvo, A.C. Chialvo, Recent progress in the kinetic analysis of the hydrogen electrode reaction in steady state, *Curr. Top. Electrochem.* 11 (2006) 1–11.
- [3] N.M. Markovic, P.N. Ross Jr., Electrocatalysis at well-defined surfaces: kinetics of oxygen reduction and hydrogen oxidation/evolution on Pt(hkl) electrodes, in: A. Wieckowski (Ed.), Interfacial Electrochemistry—Theory, Experiments, and Applications, Marcel Dekker, New York, 1999, p. 821 (Ch. 46).
- [4] M.C. Tavares, S.A.S. Machado, L.H. Mazo, Study of hydrogen evolution reaction in acid medium on Pt microelectrodes, *Electrochim. Acta* 46 (2001) 4359–4369.
- [5] P.M. Quaino, M.R. Gennero de Chialvo, A.C. Chialvo, Hydrogen electrode reaction: A complete kinetic description, *Electrochim. Acta* 52 (2007) 7396–7403.
- [6] S. Chen, A. Kucernak, Electrocatalysis under conditions of high mass transport: investigation of hydrogen oxidation on single submicron Pt particles supported on carbon, *J. Phys. Chem. B* 108 (2004) 13984–13994.
- [7] J.H. Barber, B.E. Conway, Structural specificity of the kinetics of the hydrogen evolution reaction on the low-index surfaces of Pt single-crystal electrodes in 0.5 M dm⁻³ NaOH, *J. Electroanal. Chem.* 461 (1999) 80–89.
- [8] T.J. Schmidt, P.N. Ross, N.M. Markovic Jr., Temperature dependent surface electrochemistry on Pt single crystals in alkaline electrolytes: Part 2. the hydrogen evolution/oxidation reaction, *J. Electroanal. Chem.* 524–525 (2002) 252–260.
- [9] W. Sheng, H. Gasteiger, Y. Shao-Horn, Hydrogen oxidation and evolution reaction kinetics on platinum: acid vs. alkaline electrolytes, *J. Electrochem. Soc.* 157 (2010) B1529–B1536.
- [10] W.J. Albery, Effect of the dissociation of water on electrochemical studies involving hydrogen ions, *Trans. Faraday Soc.* 62 (1966) 1575–1582.
- [11] M. Auinger, I. Katsounaros, J.C. Meier, S.O. Klemm, P. Ulrich Biedermann, A.A. Topalov, M. Rohwerder, K.J.J. Mayrhofer, Near-surface ion distribution and buffer effects during electrochemical reactions, *Phys. Chem. Chem. Phys.* 13 (2011) 16384–16394.
- [12] I. Katsounaros, J.C. Meier, S.O. Klemm, A.A. Topalov, P. Ulrich Biedermann, M. Auinger, K.J.J. Mayrhofer, The effective surface pH during reactions at the solid-liquid interface, *Electrochim. Commun.* 13 (2011) 634–637.
- [13] B.Y. Pirogov, A.G. Zelinsky, Voltammetric currents of the reduction of hydrogen ions from monoprotic acids, the effect of water dissociation, *J. Electroanal. Chem.* 593 (2006) 119–124.
- [14] S. Hessami, C.W. Tobias, In-situ measurement of interfacial pH using a rotating ring-disk electrode, *AIChE J.* 39 (1993) 149–162.
- [15] N. Zech, D. Landolt, The influence of boric acid and sulfate ions on the hydrogen formation in Ni-Fe plating electrolytes, *Electrochim. Acta* 45 (2000) 3461–3471.
- [16] S. Daniele, I. Lavagnini, M. Antonietta Baldo, F. Magno, Steady state voltammetry at microelectrodes for the hydrogen evolution from strong and weak acids under pseudo-first and second order kinetic conditions, *J. Electroanal. Chem.* 404 (1996) 105–111.
- [17] M. Ciszkowska, Z. Stojek, S.E. Morris, J.G. Osteryoung, Steady-state voltammetry of strong and weak acids with and without supporting electrolyte, *Anal. Chem.* 64 (1992) 2372–2377.
- [18] J. Zhou, Y. Zu, A.J. Bard, Scanning electrochemical microscopy—Part 39. The proton/hydrogen mediator system and its application to the study of the electrocatalysis of hydrogen oxidation, *J. Electroanal. Chem.* 491 (2000) 22–29.
- [19] S. Daniele, C. Bragato, M. Antonietta Baldo, A steady-state voltammetric procedure for the determination of hydrogen ions and total acid concentration in mixtures of a strong and a weak monoprotic acid, *Electrochim. Acta* 52 (2006) 54–61.
- [20] S. Lubetkin, The motion of electrolytic gas bubbles near electrodes, *Electrochim. Acta* 48 (2002) 357–375.
- [21] A.J. Bard, L.R. Faulkner, *Electrochemical Methods—Fundamental and applications*, 2nd ed., Wiley, New York, 2001.
- [22] V. Lazarescu, J. Clavilier, pH effects on the potentiodynamic behavior of the Pt(111) electrode in acidified NaClO₄ solutions, *Electrochim. Acta* 44 (1998) 931–941.
- [23] M.R. Gennaro de Chialvo, A.C. Chialvo, Hydrogen diffusion effects on the kinetics of the hydrogen electrode reaction. Part I. theoretical aspects, *Phys. Chem. Chem. Phys.* 6 (2004) 4009–4017.
- [24] J.L. Fernández, M.R. Gennaro de Chialvo, A.C. Chialvo, Evaluation of the kinetic parameters of the hydrogen electrode reaction from the analysis of the equilibrium polarisation resistance, *Phys. Chem. Chem. Phys.* 5 (2003) 2875–2880.
- [25] M.R. Gennaro de Chialvo, A.C. Chialvo, Kinetics of hydrogen evolution reaction with Frumkin adsorption: re-examination of the volmer-heyrovsky and volmer-tafel routes, *Electrochim. Acta* 44 (1998) 841–851.
- [26] P.M. Quaino, M.R. Gennaro de Chialvo, A.C. Chialvo, Hydrogen diffusion effects on the kinetics of the hydrogen electrode reaction: Part II. evaluation of kinetic parameters, *Phys. Chem. Chem. Phys.* 6 (2004) 4450–4455.
- [27] M.R. Gennaro de Chialvo, A.C. Chialvo, The polarisation resistance, exchange current density and stoichiometric number for the hydrogen evolution reaction: theoretical aspects, *J. Electroanal. Chem.* 415 (1996) 97–106.
- [28] H.L. Bonazza, J.L. Fernández, An efficient method for fabrication of disk-shaped scanning electrochemical microscopy probes with small glass-sheath thicknesses, *J. Electroanal. Chem.* 650 (2010) 75–81.
- [29] F.F. Fan, J.L. Fernández, B. Liu, J. Mauzeroll, C.G. Zoski, Ultramicroelectrodes—UME fabrication/characterization basics, in: C.G. Zoski (Ed.), *Handbook of Electrochemistry*, Elsevier, Amsterdam, 2007, p. 189 (Ch. 6).
- [30] R. Woods, Hydrogen adsorption on platinum, iridium and rhodium electrodes at reduced temperatures and the determination of real surface area, *J. Electroanal. Chem. Interface Electrochem.* 49 (1974) 217–226.
- [31] P.M. Quaino, J.L. Fernández, M.R. Gennaro de Chialvo, A.C. Chialvo, Hydrogen oxidation reaction on microelectrodes: analysis of the contribution of the kinetic routes, *J. Mol. Catal. A: Chem.* 252 (2006) 156–162.
- [32] M.D. Arce, J.L. Fernández, M.R. Gennaro de Chialvo, A.C. Chialvo, Fabrication, characterization and application of graphite ring ultramicroelectrodes for kinetic studies of fuel cell reactions under high mass-transport rates, *J. Electroanal. Chem.* 642 (2010) 41–51.